An Efficient and Robust Indoor Magnetic Field Matching Positioning Solution Based on Consumer-Grade IMUs for Smartphones

Jian Kuang, Taiyu Li, and Xiaoji Niu(✉)

GNSS Research Center, Wuhan University, Wuhan, China
xjniu@whu.edu.cn

Abstract. This paper proposes an indoor magnetic field matching positioning (MFMP) scheme based on consumer-grade inertial measurement units (IMUs). The proposed MFMP can efficiently generate a magnetic field map and achieve robust matching positioning without calibrating the magnetometer bias. In the magnetic field map generation stage, a pedestrian positioning and orientation system (P-POS) is employed to provide the precise position and attitude of the smartphone during the data collection, and rasterization and bilinear interpolation methods are utilized to generate a three-dimensional grid magnetic map. In the real-time positioning stage, the position and attitude generated by pedestrian dead reckoning (PDR) are used to improve the position distinguishability of the magnetic field features and obtain the transformation relationship (from the navigation frame to the sensor frame). And the differential magnetic field features in the sensor frame are used to achieve matching positioning independent of the magnetometer bias. The slight differences in the magnetic field maps based on different smartphones show that the proposed scheme can efficiently generate a high precision magnetic map. Additionally, the positioning results of multiple tests using multiple smartphones show that the proposed scheme is less affected by the magnetometer bias. Furthermore, it has similar positioning performance in different smartphones, achieving continuous and robust meter-level positioning accuracy.

Keywords: Magnetic matching · Inertial Measurement Unit (IMU) · Pedestrian Dead Reckoning (PDR) · Indoor positioning · Pedestrian navigation

1 Introduction

Due to the interference of steel materials, indoor geomagnetic field has ubiquitous distortion features in the building, which can be used for indoor positioning. Compared with the radio positioning signals (including WiFi [1], Bluetooth, 5G [2], UWB [3], etc.), magnetic field signals have the advantages of ubiquity, stability, and immunity to human body influence. Therefore, magnetic field matching positioning (MFMP) has become one of the mainstream indoor positioning methods for mass consumer application [4].

C. Yang and J. Xie (Eds.): *China Satellite Navigation Conference (CSNC 2021) Proceedings*, LNEE 773, pp. 535–545, 2021.
https://doi.org/10.1007/978-981-16-3142-9_51

MFMP includes two stages: magnetic field map generation and real-time positioning. In the magnetic field map generation stage, the correlation between the magnetic field features and the geographic coordinates with certain measurement methods is established. The walking survey (WS) is the most used method to generate a magnetic field map. For the reason that WS achieves a balance between measurement accuracy and cost comparing with the methods of the point by point and crowdsourcing [5]. Nevertheless, the measurement efficiency and accuracy of WS are still limited, which cannot meet the requirements for generating magnetic field maps in a wide range of indoor scenes.

In the real-time positioning stage, the similarity calculation between the observed and the reference magnetic field features coming from the magnetic field map is used for determining the current user's location. Dynamic time wrap (DTW) [6] and particle filter (PF) [7] are the two most frequently used methods in the published literature. However, the frequently changing magnetometer bias seriously deteriorates the performance of the above methods. Many researchers try to use the differential magnetic field features in the navigation coordinates (n-frame) to eliminate the effect of magnetometer bias [8]. Unfortunately, the projection of the magnetometer bias in the n-frame is not a fixed value, so the differential magnetic field features in the n-frame cannot achieve the purpose of eliminating the magnetometer bias.

To solve the above-mentioned typical problems of the magnetic field signals-based positioning method, this paper designs an indoor MFMP solution based on consumer-grade inertial measurement units (IMUs), which can efficiently generate a magnetic field map and achieve robust matching positioning without calibrating the magnetometer bias.

2 Overview of Magnetic Field Positioning Solution

Figure 1 shows the flow of the MFMP scheme, which can be divided into two parts: 1) Magnetic field map generation stage. A pedestrian positioning and orientation system (P-POS) is used for providing accuracy coordinates of the data collection trajectories and attitude of the smartphone, and a bilinear interpolation method is utilized to generate a

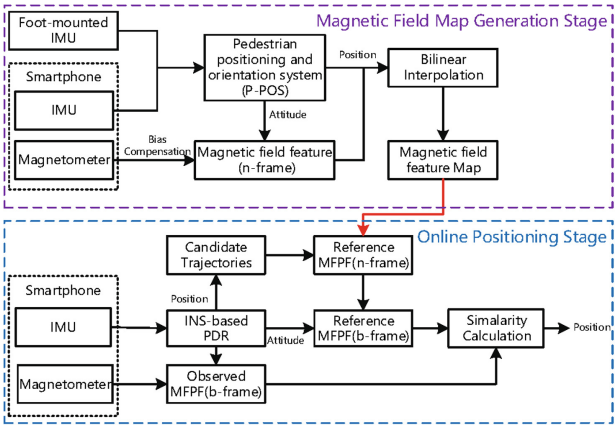

Fig. 1. The flow of the MFMP scheme based on consumer IMUs

three-dimensional grid magnetic map. 2) Online positioning stage. The relative position and attitude coming from the pedestrian dead reckoning (PDR) algorithm are used for correlating the observed magnetic field features to form the magnetic field profile to improve the position distinguishability. Additionally, the differential magnetic field profile in the sensor frame (b-frame) is used to eliminate the influence of the magnetometer bias and provide stable positioning results.

3 Magnetic Field Map Generation Stage

The magnetic field map is the basis of the matching positioning scheme. The construction and maintenance efficiency of the magnetic field map determines the cost of the entire positioning solution and the accuracy of the magnetic field map defines the upper limit of the accuracy of the MFMP method during the online positioning stage.

The test results of [9] show that P-POS can provide decimeter-level positioning and degree-level attitude when adjacent control points are separated by 50m. Inspired by this method, this paper uses the P-POS based walking survey method to collect the magnetic field map data, as shown in Fig. 2. The P-POS consists of a foot mounted IMU (Foot-IMU) and a handheld smartphone. Then, the sensor bias must be deducted from the magnetometer observation for obtaining the accurate environmental magnetic field features after data collection. The simple ellipsoid fitting method is used for estimating the magnetometer bias [10]. And the estimated attitude of the smartphone coming from P-POS are used for projecting the compensated magnetic field feature from the b-frame to the n-frame

$$\mathbf{M}^n = \mathbf{C}_b^n\left(\tilde{\mathbf{M}}^b - \mathbf{b}_m\right) \tag{1}$$

where $\mathbf{M}^n = \begin{bmatrix} m_n & m_e & m_d \end{bmatrix}^{\mathbf{T}}$ is the 3D magnetic field feature in the n-frame, including north, east and vertical components; $\tilde{\mathbf{M}}^b$ is the output of the three-axis magnetometer; $\mathbf{b}_m$ is the magnetometer bias; and $\mathbf{C}_b^n$ is directional cosine matrix from the b-frame to n-frame.

Due to the high sampling rate of the magnetometer (e.g., 100 Hz) and the uneven distribution of the reference trajectories, there are some areas that will be collected multiple times while some areas are not covered. Therefore, rasterization and interpolation are employed to generate a uniformly distributed magnetic field map.

Rasterization: 1) Generate a minimum rectangle according to the estimated coordinates of the reference trajectories, and divide the rectangle into grids of the same size. 2) The observed magnetic field features are allocated to the grid according to the estimated coordinates of the smartphone, and the magnetic field features in the same grid are averaged.

Linear interpolation: 1) Determine the position coordinates of the grid to be interpolated (e.g., grid No. 0 in Fig. 3), and set the search radius (e.g., 1m) of the effective grid. 2) Traverse the eight directions (i.e., east, south, west, north, northwest, northeast, southeast, and southwest) of grid No. 0. If the grid with a valid magnetic field feature is detected, it will return true, such as the grids numbered 1–7 in the Fig. 2. 3) Based on the objective fact that the magnetic field features can only be interpolated, the grid No.

3 will be eliminated; 4) The other valid grids are used for obtaining the magnetic field features of grid No. 0 by linear interpolation. The linear interpolation formula can be expressed as

$$\mathbf{M}_0^n = \frac{\mathbf{M}_{1,5}^n + \mathbf{M}_{2,6}^n + \mathrm{M}_{4,7}^n}{3} \tag{2}$$

where $\mathbf{M}_{i,j}^n = \frac{d_{j-0}\mathbf{M}_i^n + d_{i-0}\mathbf{M}_j^n}{d_{i-0}+d_{j-0}}$; $\mathbf{M}_i^n$ is the magnetic field feature of the i-th grid; $d_{i-0} = \sqrt{(x_i - x_0) + (y_i - y_0)}$ is the distance between the i-th grid and the 0-th grid.

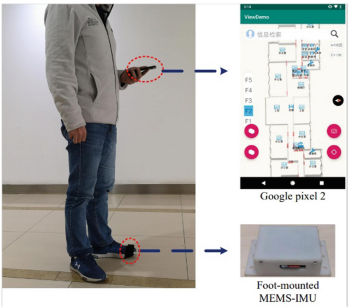

Fig. 2. The structure of the P-POS

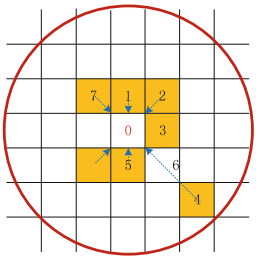

Fig. 3. Obtain a magnetic field feature by linear interpolation

4 Real-Time Positioning Stage

Because of the low dimensionality of the magnetic field feature in one position, the time series of the magnetic field features and the corresponding relative positions are correlated to form a combined feature, called the magnetic field profile (MFP). As shown in Fig. 4, the magnetic field features at the four positions (i.e., A, B, C, and D) are regard as an MFP. Because the relative spatial relationship (such as direction and distance) changes between two adjacent magnetic field features are preserved, a MFP will has a higher degree of position discrimination. Based on the relative positions and attitude angles estimated by the PDR [11, 12], an observed MFP can be expressed as

$$oMFP = \left\{ \begin{array}{c} \mathbf{r}_1^n \left(\mathbf{C}_b^n\right)_1 \tilde{\mathbf{M}}_1^b \\ \cdots \\ \mathbf{r}_k^n \left(\mathbf{C}_b^n\right)_k \tilde{\mathbf{M}}_k^b \end{array} \right\} \tag{3}$$

where $\mathbf{r}^n$ is the plane position in the n-frame, including the north and east directions; $\mathbf{C}_b^n$ is the cosine matrix of the direction from the b-frame to the n-frame, provided by the PDR; $\tilde{\mathbf{M}}^b$ is the output of the magnetometer; and k is the length of a observed MFP.

Then, the problem of MFMP can be simplified as finding the conversion relationship (i.e., translation and rotation parameters) between the relative trajectory and the absolute trajectory. However, the conversion relationship and the coordinates of the absolute

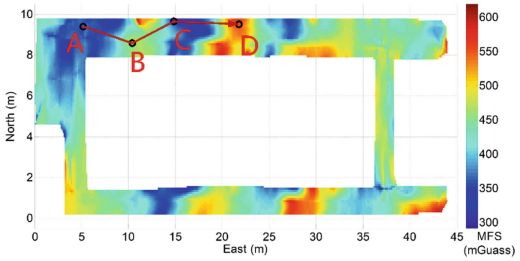

Fig. 4. Magnetic profile

trajectory are both unknown, so we cannot estimate the translation and rotation parameters by using mathematical analysis methods. An alternative approach is to generate all possible reference trajectories based on the relative trajectory by traversing possible translation and rotation parameters. Then the conversion relationship is determined according to the similarity between the observed and the reference magnetic field features corresponding to the candidate reference trajectories. Figure 5 shows the detail process of generating candidate reference trajectories. 1) Obtain the relative trajectory S based on the relative position sequence calculated by PDR, and rotate S by $\Delta\theta$ around the first point to obtain the trajectory S'. 2) Translate S by Δn in the north-south direction to obtain the trajectory S''. 3) Translate S by Δe along the east-west direction to obtain the trajectory S'''.

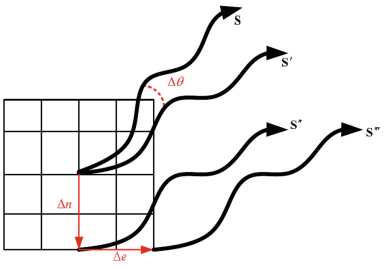

Fig. 5. The generation workflow of a candidate trajectory

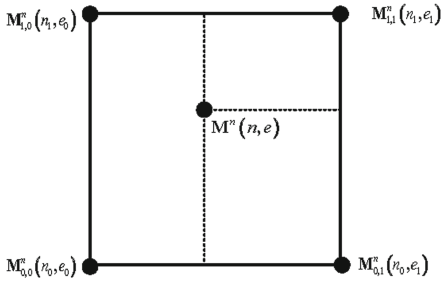

Fig. 6. Reference magnetic feature at (n, e) from the bilinear interpolation method

The candidate trajectory S''' can be expressed as:

$$\mathbf{r}_j^{n'} = C(\Delta\theta)\left(\mathbf{r}_j^n - \mathbf{r}_1^n\right) + \mathbf{r}_1^n + \Delta\mathbf{r}^n \tag{4}$$

where $\Delta\mathbf{r}^n = \left[\Delta n \ \Delta e\right]^T$, $C(\Delta\theta) = \begin{bmatrix} \cos(\Delta\theta) & -\sin(\Delta\theta) \\ \sin(\Delta\theta) & \cos(\Delta\theta) \end{bmatrix}$, $\mathbf{r}_j^{n'}$ is the coordinates of the j-th point of the candidate reference trajectory. The corresponding direction cosine matrix $\mathbf{C}_b^n$ also needs to be adjusted accordingly

$$\left(C_b^{n'}\right)_j = C_n^{n'}\left(C_b^n\right)_j \tag{5}$$

where $C_n^{n'} = \begin{bmatrix} \cos(\Delta\theta) & -\sin(\Delta\theta) & 0 \\ \sin(\Delta\theta) & \cos(\Delta\theta) & 0 \\ 0 & 0 & 1 \end{bmatrix}$, $\left(C_b^{n'}\right)_j$ is the directional cosine matrix from b-frame to n-frame corresponding to the j-th point of the candidate reference trajectory.

Since the magnetic field map is composed of uniformly distributed reference points, the sampling points of the candidate reference trajectory cannot be exactly coincident with the reference points. Therefore, the bilinear interpolation method is used to obtain the reference magnetic field features with higher resolution, as shown in Fig. 6. The corresponding reference magnetic field feature of a given point $(n\ e)$ is

$$M^n \approx \alpha_1 M_{0,1}^n + \alpha_2 M_{0,0}^n + \alpha_3 M_{1,1}^n + \alpha_4 M_{1,0}^n \tag{6}$$

where $\alpha_1 = \frac{(n_1-n)(e-e_0)}{(n_1-n_0)(e_1-e_0)}$, $\alpha_2 = \frac{(n_1-n)(e_1-e)}{(n_1-n_0)(e_1-e_0)}$, $\alpha_3 = \frac{(n-n_0)(e-e_0)}{(n_1-n_0)(e_1-e_0)}$, $\alpha_4 = \frac{(n-n_0)(e_1-e)}{(n_1-n_0)(e_1-e_0)}$. A reference MFP can be expressed as

$$rMFP = \begin{Bmatrix} r_1^{n'} \left(C_b^{n'}\right)_1 M_1^b \\ \cdots \\ r_k^{n'} \left(C_b^{n'}\right)_k M_k^b \end{Bmatrix} \tag{7}$$

where $M_1^b = \left(C_b^{n'}\right)_1^T M_1^n$ is the reference MFP in the b-frame.

Based on the characteristic that the magnetometer bias is a fixed value in the b-frame, the differential MFP in the b-frame is used for eliminating the influence of the magnetometer bias. In order to avoid large errors of the selected reference magnetic field feature, this solution performs de-averaging processing on the observed MFP and the reference MFP respectively. Then, the DTW algorithm is used to calculate the similarity between the observed MFP and the reference MFP. The DTW compresses or stretches the reference axis of the two sequences to be matched so that two sequences with different lengths have better matching results. This will help solve the problem that the PDR algorithm cannot accurately estimate the pedestrian step length.

5 Test Results and Analysis

The test is conducted in a typical office building scene with a size of about 94 m × 22 m. Figure 6 shows the indoor structure where the red box is the test area (Fig. 7).

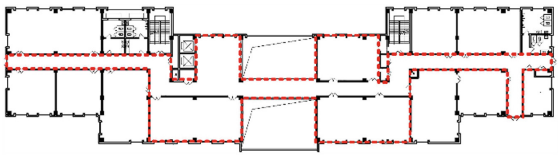

Fig. 7. Indoor structure of the test scene

In the magnetic field map generation stage, testers use a P-POS (Fig. 2) to provide high precision position and attitude of the smartphone. And the system time of the

smartphone and Foot-IMU is aligned via Bluetooth communication. In addition, in order to evaluate the performance of real-time magnetic field matching positioning algorithm, the positioning accuracy evaluation in this paper is performed in offline mode.

Three smartphones (Google pixel2, pixel3 and Mi8) are employed to generate the magnetic field map of the test area, which takes 800 s, 825 s, and 770 s respectively. The effective area is about 500 m^2, so the average data collection efficiency of the magnetic field map is about 37 m^2/min. If the tester follows the "#" path at a speed of 1.2 m/s in an indoor open area of 100 m^2, the data collection efficiency will reach 55 m^2/min.

Figure 8 shows the Google pixel2-based magnetic field map. The horizontal and vertical axes are east and north positions respectively, and the colors represent the values of the magnetic field feature. Subgraphs (a)– (c) are the north, east and vertical, respectively. The magnetic field features of the adjacent geographic locations has a gentle transition, which is consistent with objective physical phenomena. Figure 9 shows the difference between the magnetic field map Mi8 and Google pixel2. The differences in most areas are distributed around 0. We learn that the P-POS provides position and attitude angle with good repeatability which can meet the requirements of generating a magnetic field map. In addition, the difference in magnetic field features in some areas reached about 100 milligauss (mGauss). The reason is that the accuracy of P-POS is limited (which is at about decimeter level). the magnetic field feature decay with the 3rd power of the spatial distance, small position and attitude errors will cause obvious magnetic field feature deviation near the magnetic field interference source.

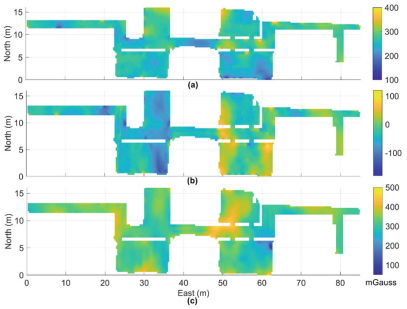

Fig. 8. Magnetic field map based on Google pixel2. (a) north, (b) east, (c) vertical

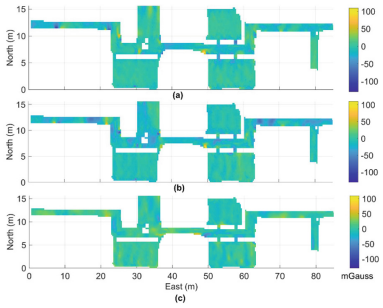

Fig. 9. The difference of magnetic field maps based on Mi 8 and Google pixel2. (a) north, (b) east, (c) vertical.

Figure 10 shows the probability density function of the difference of the magnetic field map different smartphones. Table 1 summarizes the root mean square (RMS), 68% and 95% of the difference of the magnetic field maps based on different smartphones. The difference in the three directions of the magnetic field maps based on any two smartphones is less than 20 mGauss (RMS), and 95% of the difference is less than 40 mGauss. Compared with the noise level of magnetometers built in most smartphones is about 10–20 mGauss, and the errors caused by P-POS and map generation algorithms are very small. Therefore, the magnetic field map generation method designed in this paper is highly efficient and precise.

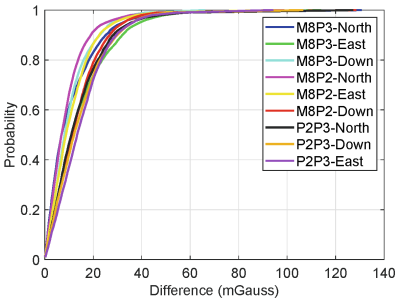

Fig. 10. The cumulative density function of the difference of two magnetic field maps

Table 1. Root mean square, 68% and 95% of the difference in magnetic field maps of different smartphones (unit: milligauss)

	Mi8- Pixel3		Mi8-Pixel2		Pixel2-Pixel3	
	RMS	68%/95%	RMS	68%/95%	RMS	68%/95%
北	16.0	12.1/32.3	13.0	10.1/25.2	18.4	16.2/35.6
东	19.4	16.7/39.1	14.7	13.1/28.7	19.1	18.3/36.3
垂	13.6	11.6/27.7	17.0	15.8/32.6	18.4	17.6/36.2

Based on the magnetic field map of Pixel2, we conducted 8 tests using 4 different smartphones (Honor V10, Google Pixel2, Pixel3, and Mi8). As the proposed algorithm does not need to calibrate the magnetometer bias, the real-time positioning algorithm evaluation stage will no longer perform bias compensation on the magnetometer observations. Because the magnetic field feature matching method does not have the global positioning ability and cannot quickly complete the autonomous initialization of the system state, MFMP usually used as an auxiliary positioning method. Here, the initial position is manually given, and WiFi/Bluetooth can be used to give a rough position (such as the position error is less than 10 m) for the real-time positioning program.

Figure 11 shows the trajectories of 8 tests of the 4 smartphones. The red line is the reference trajectory given by P-POS; the blue line is the trajectory of PDR, and the green line is the trajectory of MFMP. The sub-pictures (a) and (b) correspond to Honor V10; (c) and (d) correspond to Google Pixel3; (e) and (f) correspond to Mi 8, (g) and (h) correspond to Google Pixel2. The trajectories generated by the PDR in different tests have different scale and deformation error, and the trajectories of MFMP have a good coincidence with the reference trajectories.

Figure 12 shows the cumulative density function of position error of the 8 tests. "V10-1" is the first test of Honor V10. The positioning errors are relatively concentrated and most of which are within 1.5 m. Figure 13 shows the magnetometer bias estimated by each of the 8 tests, where "T1-x" is the bias of the x-axis of the magnetometer in the first test. It can be observed that the magnetometer bias has arrived hundreds or even thousands of mGauss, with a fluctuation of tens of mGauss. Table 2 lists the RMS, 68%

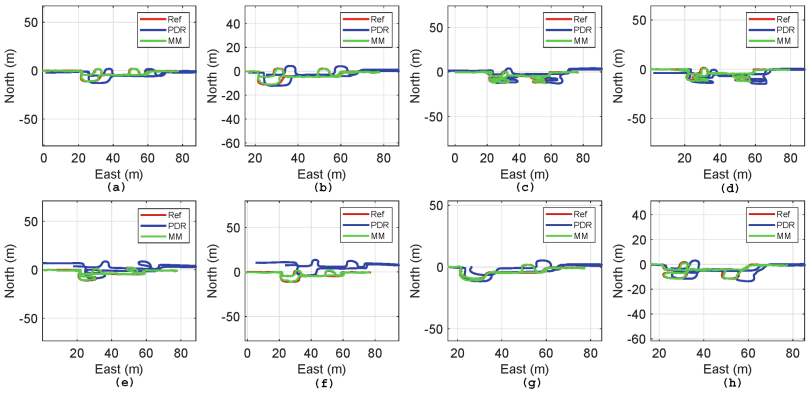

Fig. 11. The trajectories of 8 tests using 4 smartphones. (a) and (b) correspond to Honor V10, (c) and (d) correspond to Google Pixel3, (e) and (f) correspond to Mi 8, (g) and (h) correspond to Google Pixel2

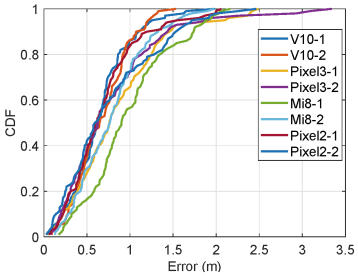

Fig. 12. Cumulative density function of position error of 8 tests

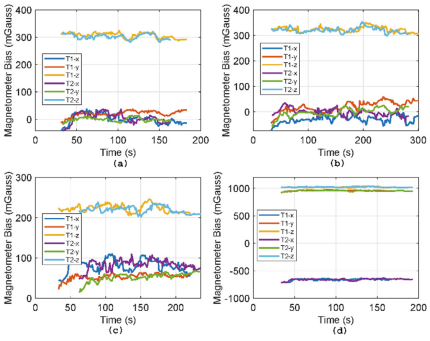

Fig. 13. The estimated magnetometer bias.

and 95% of the positioning error of the 8 tests. The RMS of the positioning errors of the 8 tests were distributed between 0.67 and 1.01 m, and the floating range was 0.34 m. Comparing with the length of a pedestrian step (about 0.6 m), the fluctuation range of the positioning error is small.

Table 2. RMS: 68% and 95% of positioning error of 8 tests (unit: m)

Test	V10-1	V10-2	Pix3-1	Pix3-2	Mi8-1	Mi8-2	Pix2-1	Pix2-1	Mean
RMS	0.67	0.79	1.01	0.99	0.78	0.87	0.74	0.84	0.83
68%	0.66	0.74	1.00	0.88	0.78	0.86	0.70	0.72	0.79
95%	1.27	1.53	2.10	1.89	1.48	1.43	1.32	1.77	1.60

In summary, although the magnetometer bias reaches thousands of mGauss and the fluctuation range reaches tens of mGauss, it has no obvious influence on the matching algorithm in this study. It can be learned that the proposed MFMP algorithm is not sensitive to the magnetometer bias, and the positioning performance difference between multiple smartphones is also small. In addition, the average positioning error of the 8 tests is 0.83 m (RMS), showing that the proposed method can reach the meter-level/sub-meter-level positioning in office buildings.

6 Conclusion and Outlook

This study has greatly improved the relative positioning and attitude estimation ability of the consumer-grade IMUs by using the constraint information formed by the pedestrian movement characteristics. The magnetic field map construction efficiency and real-time positioning stability have consequently been enhanced.

In the magnetic field map generation stage, a P-POS is used to provide decimeter-level positioning and degree-level attitude (including roll, pitch and heading) of the smartphone. The test results of using three types of smartphones to generate magnetic field maps show that the data collection efficiency of the proposed method has reached 37 m^2/min, and the difference of the magnetic field maps based on different smartphones is less than 20 mGauss (RMS).

In the real-time positioning stage, the position and attitude provided by PDR are used to improve the position distinguishability of the magnetic field feature and obtain the transformation relationship from the navigation frame to the sensor frame, so the differential MFP in the b-frame can be used for eliminating the impact of the magnetometer bias. The results of the 8 field tests of 4 smartphones show that the positioning error is distributed between 0.67 and 1.01 m, reaching an average positioning performance of 0.83 m (RMS). The experimental results have completely verified that the MFMP method designed in this study is less affected by the magnetometer bias, and there is no significant difference in positioning performance between different smart phone terminals.

Because the smartphone indoor MFMP scheme proposed in this study is highly dependent on the stability of the PDR., we will focus on automatically monitoring the integrity of the PDR and adapting it to a variety of typical smartphone usage modes in the future, such as texting, calling, and swinging. More, we will explore the method of generating magnetic field maps based on crowdsourced data to further reduce the cost of system.

References

1. Zhuang, Y., El-Sheimy, N.: Tightly-coupled integration of WiFi and MEMS sensors on handheld devices for indoor pedestrian navigation. IEEE Sens. J. **16**(1), 224–234 (2015)
2. Liu, J., Gao, K., Guo, W., Cui, J., Guo, C.: Role, path, and vision of "5G + BDS/GNSS." Satell. Navig. **1**(1), 23 (2020)
3. Van Herbruggen, B., et al.: Wi-PoS: a low-cost, open source ultra-wideband (UWB) hardware platform with long range sub-GHz backbone. Sens. Basel **19**(7), 1548 (2019)

4. Kuang, J., Niu, X., Zhang, P., Chen, X.: Indoor positioning based on pedestrian dead reckoning and magnetic field matching for smartphones. Sens. Basel **18**(12), 4142 (2018)
5. Li, Y.: Integration of MEMS Sensors, WiFi, and Magnetic Features for Indoor Pedestrian Navigation with Consumer Portable Devices. University of Calgary (2016)
6. Subbu, K.P., Gozick, B., Dantu, R.: Locate me-magnetic fields based indoor localization using smartphones. ACM Trans. Intell. Syst. Technol. **4**(4), 1–27 (2013)
7. Haverinen, J., Kemppainen, A.: Global indoor self-localization based on the ambient magnetic field. Robot. Auton. Syst. **57**, 1028–1035 (2009)
8. Kim, B., Kong, S.: Indoor positioning based on Bayesian filter using magnetometer measurement difference. In: IEEE Vehicular Technology Conference Proceedings (2015)
9. Niu, X., Liu, T., Kuang, J., Li, Y.: A novel position and orientation system for pedestrian indoor mobile mapping system. IEEE Sens. J. **21**(2), 2104–2114 (2020)
10. Tabatabaei, S.A.H., Gluhak, A., Tafazolli, R.: A Fast calibration method for Triaxial magnetometers. IEEE Trans. Inst. Meas. **62**(11), 2929–2937 (2013)
11. Kuang, J., Niu, X., Chen, X.: Robust pedestrian dead reckoning based on MEMS-IMU for smartphones. Sens. Basel **18**(5), 1391 (2018)
12. Liu, T., Niu, X., Kuang, J., Cao, S., Zhang, L., Chen, X.: Doppler shift mitigation in acoustic positioning based on pedestrian dead reckoning for smartphone. IEEE Trans. Instrum. Meas. **70**, 1–11 (2020)